4. PARAMETRIC UNCERTAINTY ANALYSIS

The purpose of the parametric uncertainty analysis is to identify which parameters are important to treat as uncertain in the flow and transport modeling. As previously discussed, uncertainty in parameter values and the need to include that uncertainty in the risk assessment prohibit a deterministic approach to the modeling. Despite this, if uncertainty in a given parameter has a minimal impact on the results, the value of including it in the Monte Carlo process is outweighed by the additional computational effort. To optimize the modeling process, a parametric uncertainty analysis was performed to identify which parameters to carry forward as uncertain and which to set as constant, best estimate, values. This analysis was performed for the Milrow site. Though the different locations of the three test cavities relative to the transition zone might be expected to lead to somewhat different results, the final parameters identified as important for Milrow coincide with those expected to be most important based on hydrogeologic principles.

The processes evaluated through their flow and transport parameters include recharge, saltwater intrusion, radionuclide transport, glass dissolution, and matrix diffusion. The end result of this analysis is a relative comparison of the effect of uncertainty of each individual parameter on the final transport results in terms of the arrival time of mass of radionuclides crossing the seafloor. First to be considered is the density-driven flow problem associated with saltwater intrusion, and the parameters affecting this process are denoted as the flow parameters. Second is the radioactive transport problem, where the movement of radionuclides from the test cavity to the seafloor is studied and the parameters of concern in this process are denoted as transport parameters.

4.1 Sensitivity/Uncertainty Analysis of Flow Parameters

The parameters of concern here are the hydraulic conductivity, K, the recharge, *Rech*, and the longitudinal and transverse macrodispersivities, A_L and A_T. Since the saltwater intrusion problem encounters a density-driven flow, the macrodispersivities are considered as flow parameters. In addition, the porosity is also considered at this stage as the spatial variability of porosity between the chimney and the surrounding area affects the solution of the saltwater intrusion problem. In all cases, the flow and the advection-dispersion equations are solved simultaneously until a steady-state condition is reached. The solution provides the groundwater velocities and the concentration distribution that can be used to identify the location and thickness of the transition zone. For each of the four parameters, a random distribution of 100 values below and above a "mean" value close to the calibration result is generated. Figure 4.1 shows the histograms for *Rech*, K, θ, and A_L. The transverse macrodispersivity, A_T, is taken as $A_L/10$, as is commonly assumed in transport modeling. As can be seen from the figure, the distribution of random recharge values covers a range of values extending from one-fourth the calibrated value to about double that value. A lognormal distribution was used to generate the recharge values and the distribution was truncated such that the upper and lower limits lead to reasonable transition zone movement around the location indicated by the chemistry data. From the 100 random values, the minimum recharge value is about 0.328 cm/year and the maximum is about 2.205 cm/year. This range lies within the recharge estimates obtained using temperature logs as discussed in Section 2.6.1.

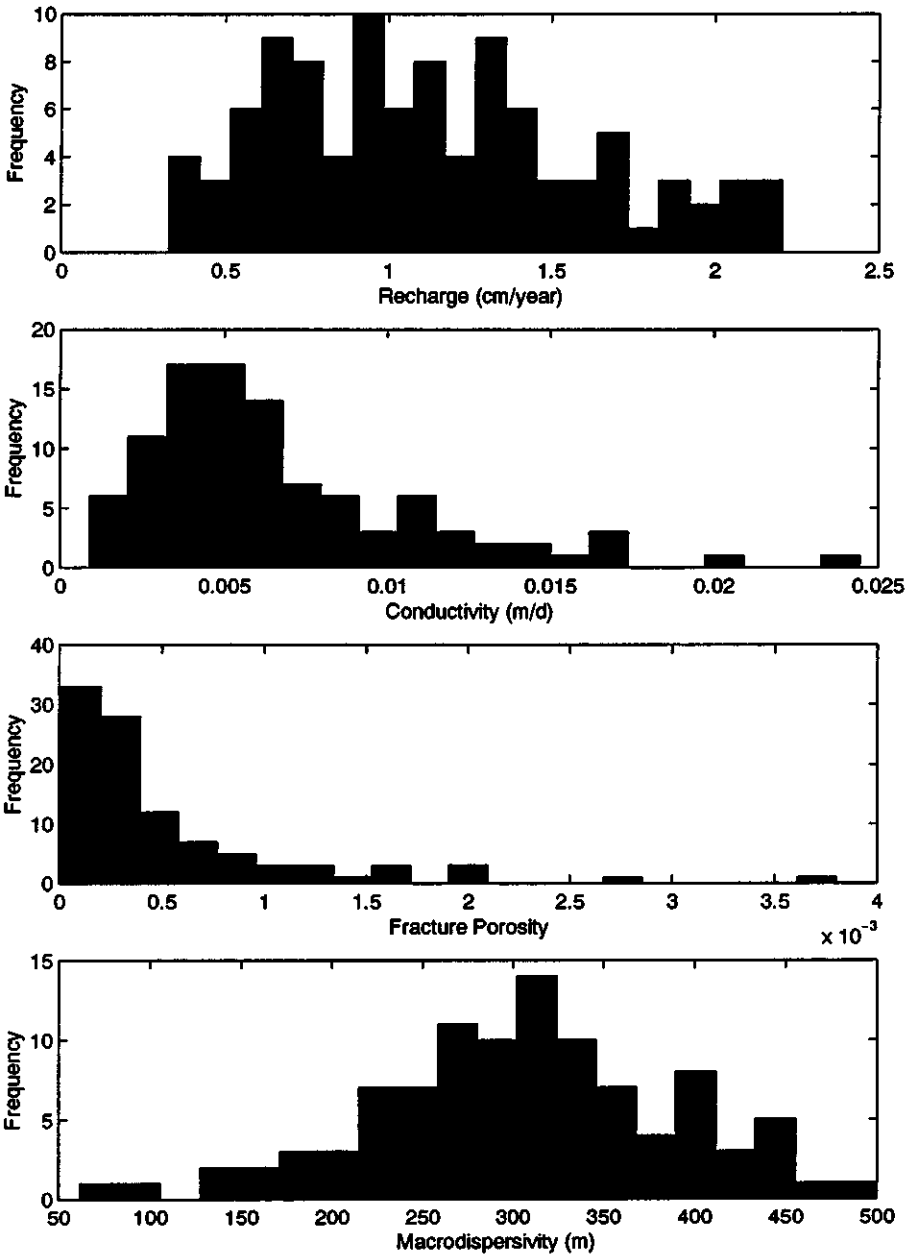

Figure 4.1. Randomly generated distributions for the parameters governing the solution to the flow problem. These distributions are used for the individual-parameter uncertainty analysis.

The uncertain conductivity values are generated from a lognormal distribution and have a mean value of 6.773×10^{-3} m/day, which is equivalent to the Milrow calibration value and it also lies between the geometric and arithmetic means of the conductivity data. These means for the full data set are 1.862×10^{-3} and 1.137×10^{-2} m/day, respectively. If an average value is computed for each of the six wells, these mean values become 1.9953×10^{-3} and 1.575×10^{-2} m/day. In both cases, the mean of the generated random distribution lies between the geometric and the arithmetic means. The maximum conductivity value among the generated 100 values is 2.445×10^{-2} m/day, whereas the minimum value is 1.5×10^{-3} m/day. This range is considered sufficient to yield realistic results. That is, by changing the uniform K value applied to the whole domain based on this distribution and keeping all the other parameters fixed, the resulting transition zone lies within the simulation domain. It should be mentioned here that values of conductivity beyond this range yield transition zones far from the one identified from the chemical data. For example, any conductivity value smaller than 1.5×10^{-3} m/day (with all other parameters fixed at their calibrated values) yields a transition zone depth greater than 2,000 m, which is more than double the depth indicated by the data (about 850 m).

From these conductivity limits and those of the recharge, the recharge-conductivity ratio is changing from 1.26×10^{-3} to 2.05×10^{-2} for the conductivity sensitivity values, and from 1.35×10^{-3} to 9.05×10^{-3} for the recharge sensitivity case. In both cases, the range of this ratio encompasses the estimate of 6.88×10^{-3} obtained by Wheatcraft (1995). However, the recharge and conductivity values considered in that study were about one order of magnitude larger than the values used here. It should be mentioned here that the recharge-conductivity ratio is the factor that controls the location of the transition zone, but the magnitude of the velocity depends on the recharge and conductivity values.

The large macrodispersivity values are considered to account for the additional mixing resulting from spatial variability that is not considered in the model. Although the base-case value chosen for longitudinal macrodispersivity is about 100 m, the mean of the distribution shown in Figure 4.1 is 300 m. This is done mainly to avoid violation of the Peclet number when small macrodispersivity values are used. Based on the distribution shown, the macrodispersivity values are taken between a minimum of 60 m and a maximum of 500 m. As mentioned earlier, the macrodispersivity changes the width of the transition zone, which affects the flow pattern and the location of the converging flow towards the seafloor.

Porosity in the cavity and chimney is assumed to be higher than the rest of the simulation domain. For all cases considered in this study, the chimney and cavity porosity is set to a fixed value of 0.07 as discussed earlier. The rest of the domain is assigned a fracture porosity value that is obtained from the random distribution generated for the fracture porosity. The random distribution of the porosity gives a minimum value of about 1.294×10^{-5} and a maximum value of 3.8×10^{-3}. The mean of the 100-value random distribution is about 5.2×10^{-4}.

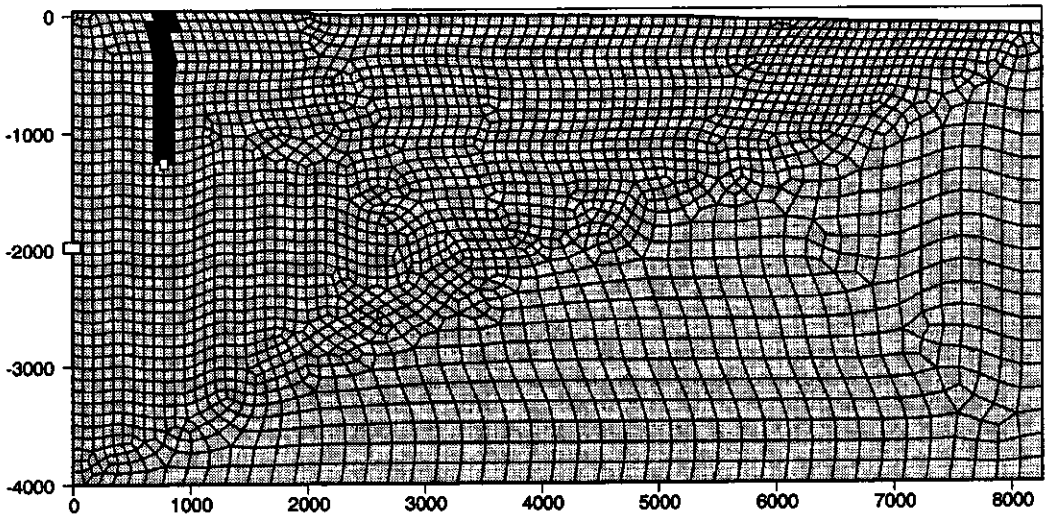

Figure 4.2. Finite-element mesh with the upper left half of the domain refined and chimney location highlighted.

4.1.1 Numerical Approach for the Parametric Uncertainty Analysis

Having generated these individual random distributions for each of the parameters considered, the variable-fluid-density groundwater flow problem is solved using FEFLOW. A new mesh is generated that is different from the one shown in Figure 2.8. The mesh remains refined in the entire left upper triangle of the simulation domain since the transition zone varies a lot with the random parameters selected. Therefore, a grid size of about 100 m is used in the upper left half of the domain and a 200-m grid is used in the lower right half (Figure 4.2). The 100-m grid size is consistent with the scale of the hydraulic and chemistry data, which were collected from straddle-packed intervals having an average length of 85 m. Figure 4.2 also shows the location of the cavity and chimney. The chimney is assumed to extend all the way up to ground surface, to account for near-surface fractures due to spalling and disruption from the surface collapse. Porosity and conductivity in the cavity and chimney are different from the rest of the domain as mentioned earlier.

The FEFLOW code deals with the flow and saltwater transport problems simultaneously in a transient mode. The transient solution continues for a certain number of time steps determined by the user. In simulations, a steady-state velocity distribution is assumed, and as such FEFLOW runs for a large number of time steps to reach steady state. A very large simulation time is implemented for all realizations considered. However, FEFLOW has an automatic time step configuration algorithm that allows for increasing the size of the time step when the changes in the flow solution are slow and the system is approaching steady state. At the beginning of the simulation, the size of the time step is very small, but it gradually increases as the solution approaches steady state. For each individual realization, the head and concentration values are monitored at a number of points within and around the transition zone as a function of time. If at the end of the simulation time the head and

concentration do not reach constant values, the simulation is repeated with a longer time until steady state is reached. This guarantees that all the runs reach steady state and that the obtained solution is stable and representative of the equilibrium state of the system.

4.1.2 Sensitivity of Concentration and Head Distributions to Flow Parameter Uncertainty

For each one of the four parameters considered, a set of 100 velocity and concentration distributions is obtained that corresponds to the 100 random input values. For the simulated head and concentration values at UAe-2, the mean of the 100 realizations as well as the standard deviation of the result are computed. Figure 4.3 through Figure 4.6 show the sensitivity of the concentration and head to the recharge, conductivity, porosity and macrodispersivity. In each figure, the mean of the Monte Carlo runs, the mean $\pm$ one standard deviation, the base-case (all parameters take their mean values) result, and the data points are plotted. Figure 4.3 shows the sensitivity of concentration and head profiles to changes in the recharge values. The one standard deviation confidence interval around the mean captures most of the data points for concentration and for head measurements. The conductivity case (Figure 4.4) covers the high concentration data (saltwater side) but gives lower concentrations than the data for the freshwater side of the transition zone. The head sensitivity to conductivity variability shown in Figure 4.4 indicates that the confidence interval encompasses all the head data at UAe-2.

It should be mentioned here that the base-case results are different than those shown in Figure 2.15 and Figure 2.16 of the calibration results (the dashed lines on those figures). This is due to adding the chimney effect, which is not present in the pre-test calibration analysis. It is assumed that the cavity and chimney are isotropic, which means that the vertical conductivity is 10 times larger than the surrounding area. In addition, the porosity in the cavity and chimney is kept in all realizations at a value of 0.07, even when the fracture porosity is drawn randomly from its assumed distribution. This leads to a base-case result that is different from the one established from calibration. The other aspect to discuss here is the use of the pre-test data for this comparison. It is evident that incorporating the cavity and chimney conditions only slightly changes the head and concentration profiles at UAe-2. Therefore, the pre-test data can still be considered as providing guidelines for choosing the model parameters and controlling the range of variability around the base-case values. The assumptions employed in this analysis are that the short-term effects of the nuclear test are neglected as the long-term behavior of the radionuclides is controlled by the steady-state conditions of the island. The only long-term effects considered are the porosity and conductivity changes in the cavity and chimney.

Figure 4.5 shows the effect of the fracture porosity parametric uncertainty on the resulting heads and concentrations at UAe-2. As expected, the porosity does not affect the solution of the flow problem even with the chimney having a different porosity. The porosity only influences the speed at which the system converges to steady state and as such, simulated heads and concentrations at UAe-2 do not show any sensitivity to the fracture porosity value outside the chimney. It should be remembered that the fracture porosity outside the chimney and cavity area will have a dramatic effect on travel times and radioactive decay of mass released from the cavity and migrating toward

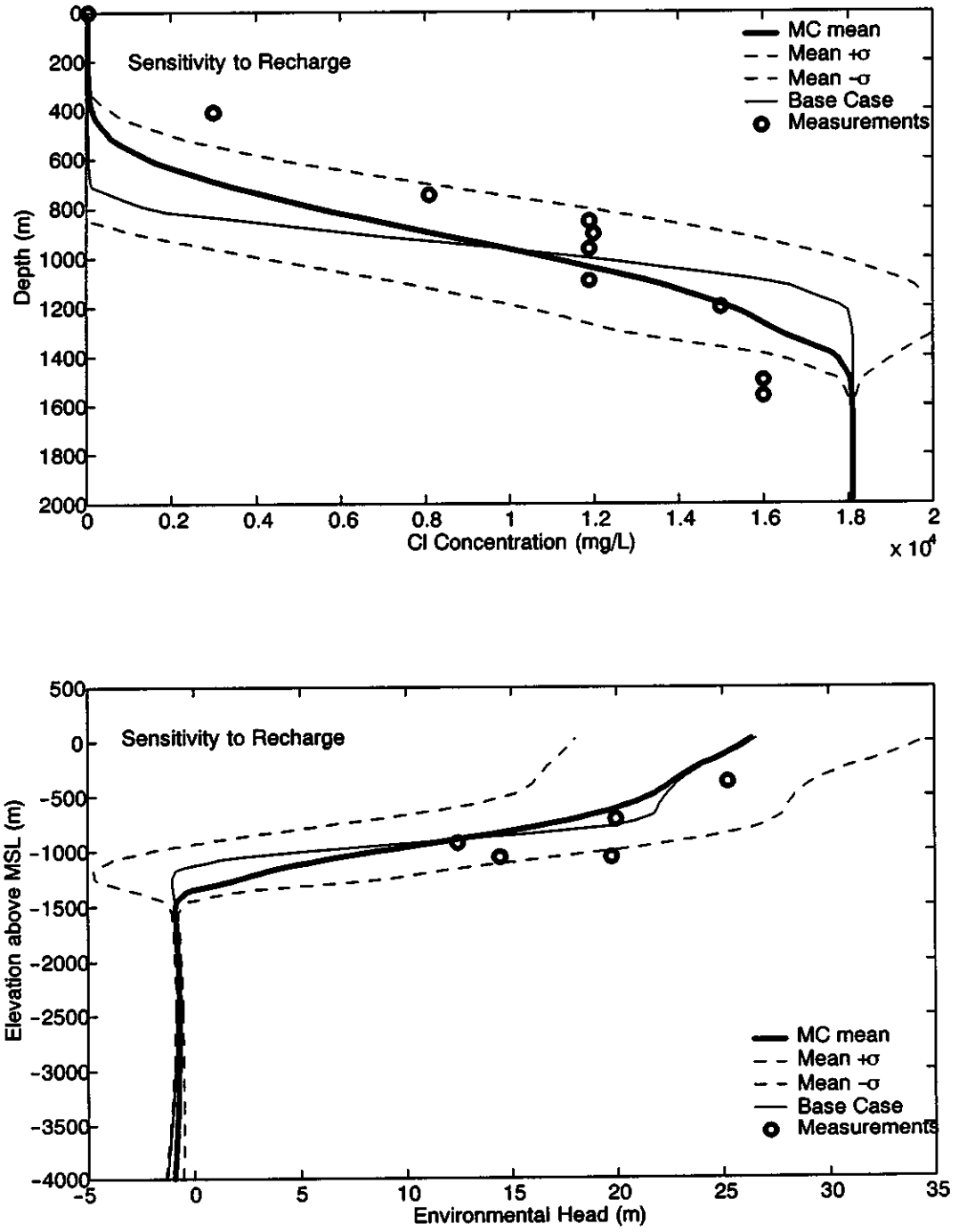

Figure 4.3. Sensitivity of UAe-2 concentration and heads to recharge in the first modeling stage.

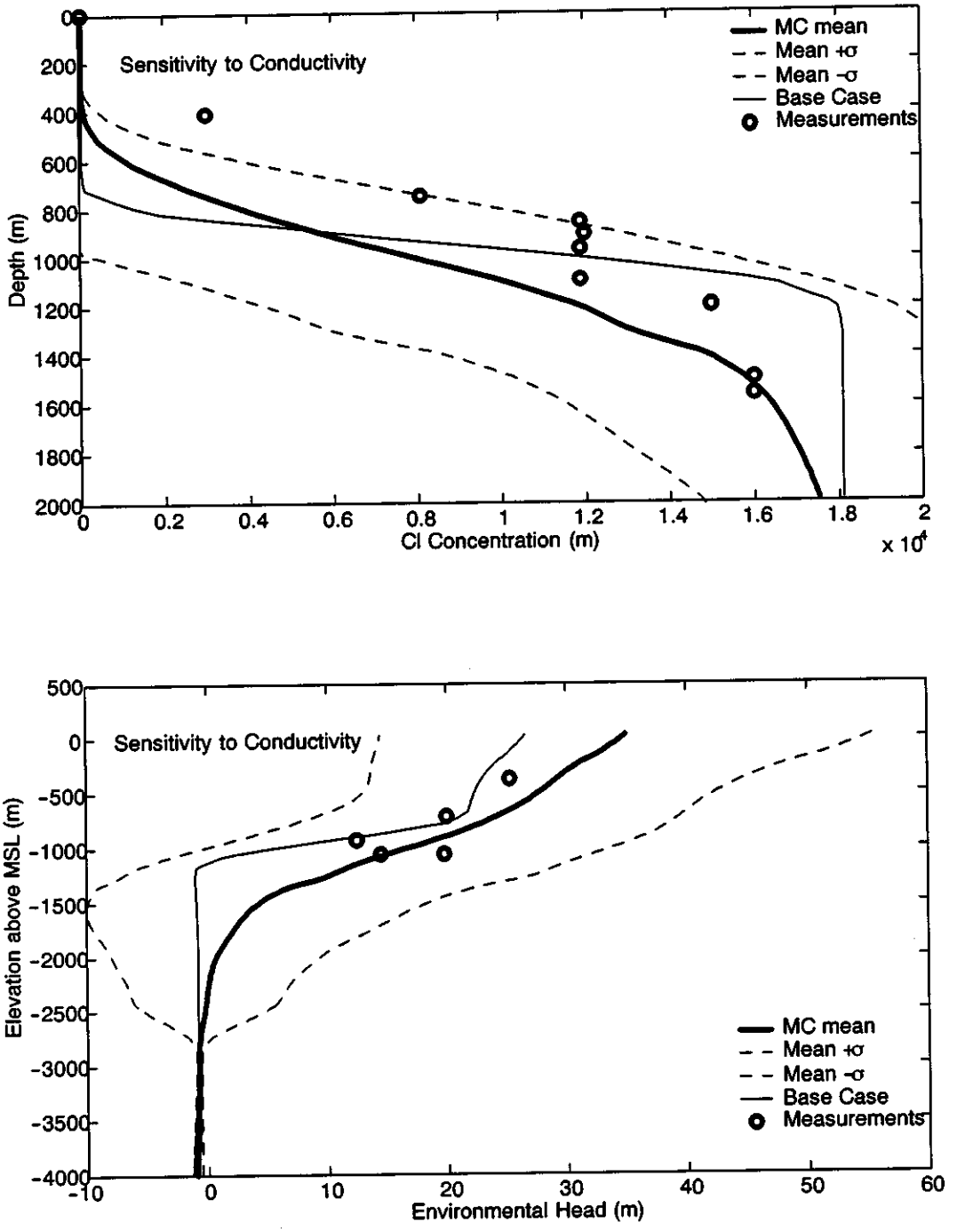

Figure 4.4. Sensitivity of UAe-2 concentration and heads to conductivity in the first modeling stage.

the seafloor. This will be demonstrated later when the effect of these parameters on travel times is analyzed.

The macrodispersivity effect is displayed in Figure 4.6. The macrodispersivity range of 60 m to 500 m considered in this sensitivity case has a minor effect on the head and concentration at UAe-2, especially at the center of the transition zone. This is to be expected since macrodispersivity leads to more or less dispersion around the center of the transition zone. Again, the final decision as to whether the changes in macrodispersivity would be important to include in the final modeling stage cannot be determined from these results. The criterion for selecting the most influential parameters is determined by analyzing the transport results in terms of travel times from the cavity to the seafloor and location where breakthrough occurs. The set of figures discussed here indicates that the simulated heads and concentrations at UAe-2 are most sensitive to conductivity and recharge and least sensitive to fracture porosity outside the chimney and macrodispersivity. This picture may be confirmed or changed by analyzing the travel time statistics for particles originating from the cavity and breaking through the seafloor.

The output of this stage is a set of 100 velocity realizations for each of the four parameters considered. These velocity realizations are used to model the radionuclide transport from the cavity toward the seafloor. The transport parameters are kept fixed at their means while addressing the effect of the four parameters that change the flow regime. When the effect of transport parameters, such as matrix diffusion coefficient, glass dissolution rate, etc., is studied, a single velocity realization with the flow parameters fixed at the calibration values is used. The following section presents the uncertainty analysis for the transport parameters. Following that discussion, the results of the parametric uncertainty analysis for both the flow and transport parameters are presented.

4.2 Sensitivity/Uncertainty Analysis of Transport Parameters

In transport simulations where the radionuclides are divided among surface-deposited nuclides and volume-deposited nuclides trapped in puddle glass, the dissolution rate, k_g, becomes an important factor affecting transport results. However, there exists a large degree of uncertainty in estimating this parameter, which leads to a couple of orders of magnitude range for the release rate. To analyze the effect of this uncertainty on transport results, a 100-value random distribution of variability for k_g ranging from 1.56×10^{-8} days^{-1} to 2.54×10^{-6} days^{-1} with a mean of about 2.44×10^{-7} days^{-1} is generated from a lognormal distribution. Figure 4.7 shows a histogram of the random distribution used in the sensitivity analysis (top) and how the release of nuclides from the puddle glass is influenced by this range of variability (bottom). This analysis is performed using a single flow realization and the transport simulations are performed for 100 different *kg* values.

A similar analysis is performed to analyze the effect of the local dispersivity, α_L. An important point here is that the macro/local dispersivity is used in both the flow and transport simulations. Since flow simulations involved solving the saltwater intrusion problem, the macrodispersivity values were used in the analysis of flow parameters. However, these macrodispersivity values were chosen to be very large for a number of reasons. First, FEFLOW solves the flow and transport equations using a finite-element technique. A Peclet number criterion has to be met for a stable

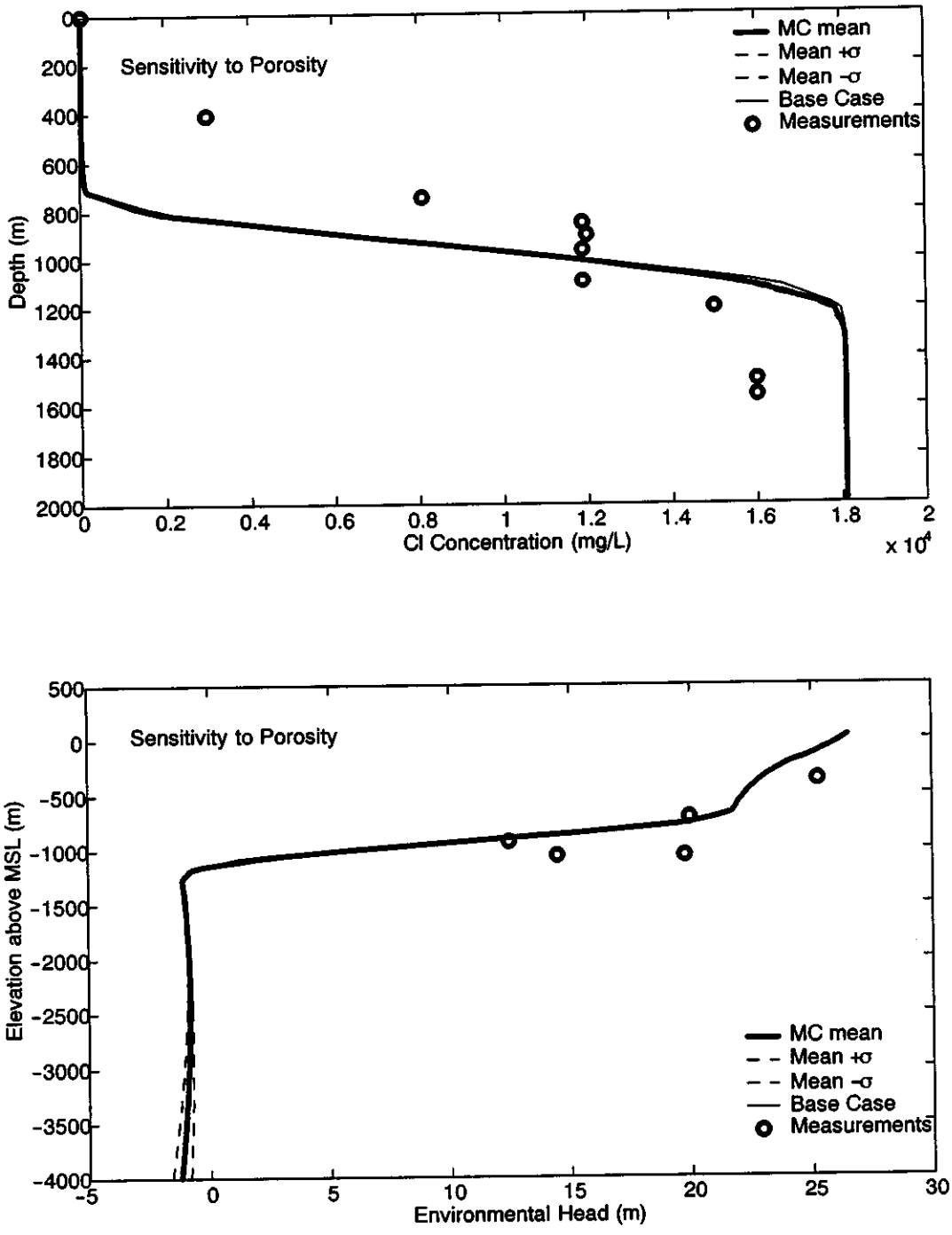

Figure 4.5. Sensitivity of UAe-2 concentration and heads to porosity in the first modeling stage.

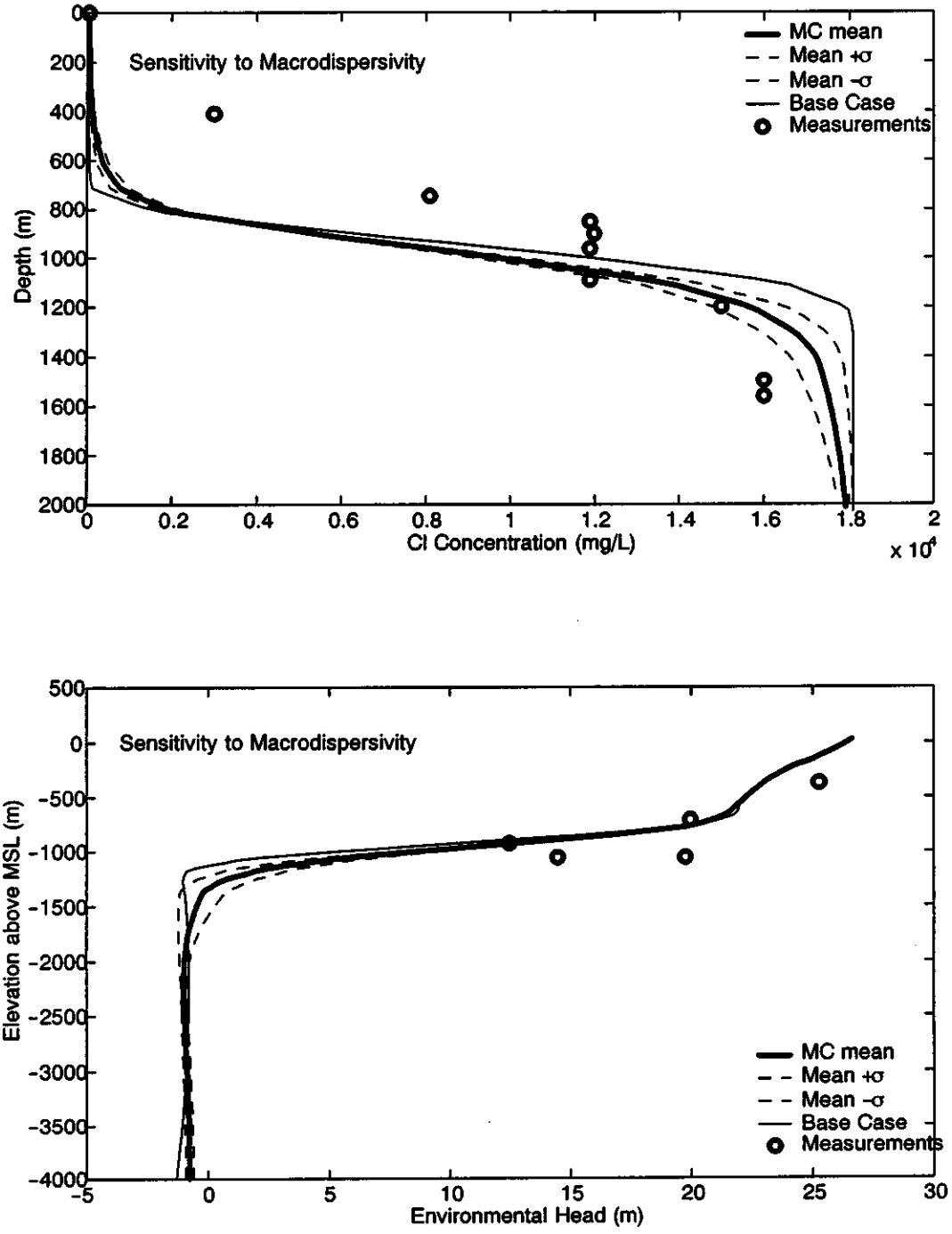

Figure 4.6. Sensitivity of UAe-2 concentration and heads to macrodispersivity in the first modeling stage.

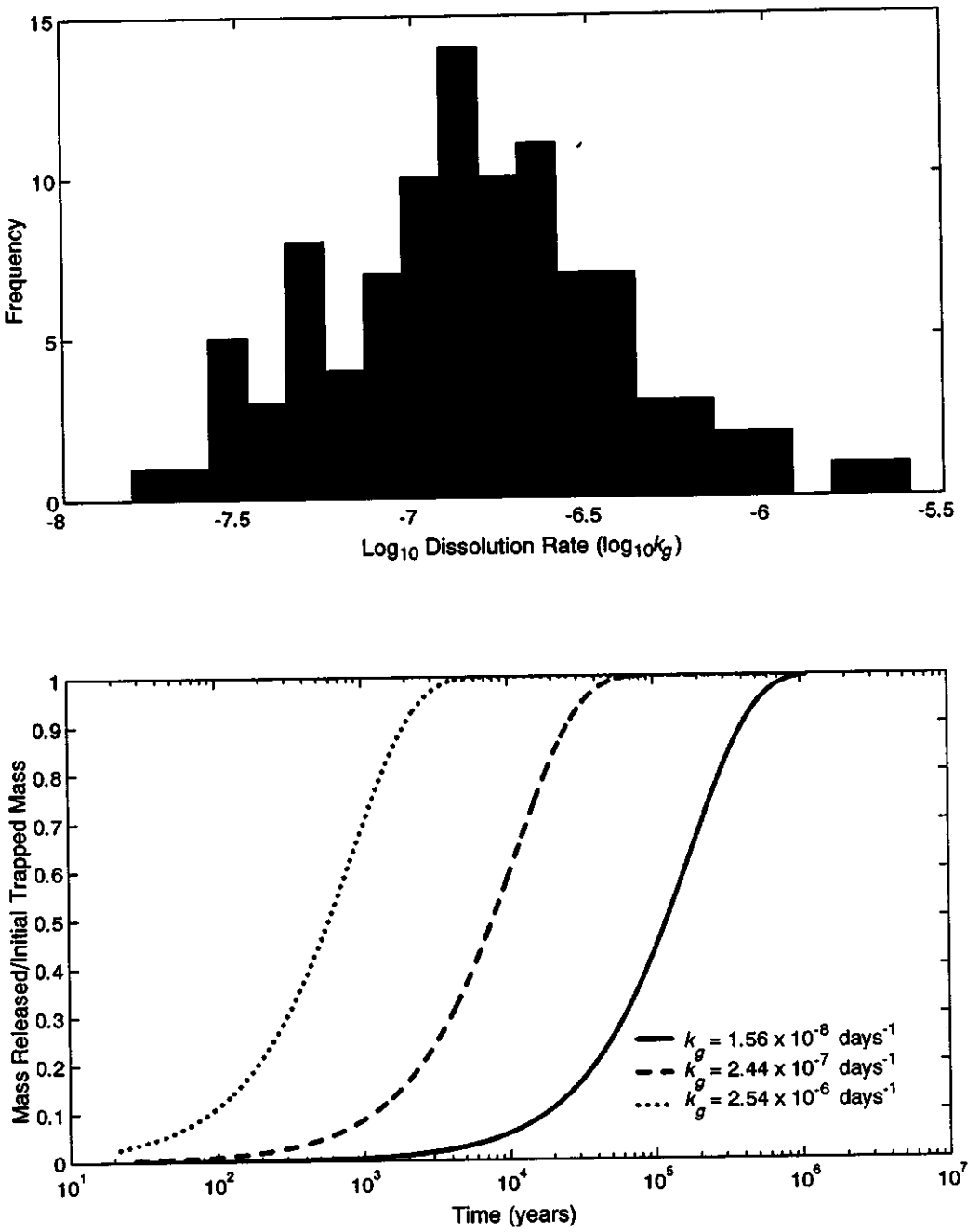

Figure 4.7. Randomly generated distribution for the glass dissolution rate, *kg* (top), and the percentage of mass released as a function of time for the minimum, mean, and maximum *kg* (bottom).

finite-element solution. The Peclet number, P_e, associated with the finite-element solutions to the advection-dispersion equation can be approximated by the ratio $(V\Delta x) / (A_L V) = (\Delta x) / (A_L)$. To obtain a stable solution when using an implicit finite-element scheme, the Peclet number should be kept less than unity and thus a very fine grid would be needed for small values of longitudinal macrodispersivity A_L. This becomes prohibitive in terms of storage and CPU time due to the large extent of the simulation domain (8,000 m x 4,000 m). Therefore, the longitudinal macrodispersivity is chosen very large to ensure a stable solution over a grid of an average size of about 100 m. The second reason for choosing such large macrodispersivities in the flow simulations is the fact that chemistry data show a largely dispersed transition zone which we tried to reproduce during calibration. It is also important to remember that no spatial variability is included in the medium conductivity, which usually adds a macro-dispersion effect to the transition zone spreading. A large macrodispersivity value may be used as a surrogate to spatial variability in hydraulic conductivity (*e.g.*, Gelhar and Axness, 1983; Hess *et al.*, 1992). For all these reasons, a large asymptotic macrodispersivity is used in flow simulations with a range extending from 60 m to 500 m as discussed earlier.

Although the dispersivity is a porous medium property, the dispersivity values used in transport simulations are chosen much smaller than those used in the saltwater intrusion problem. The reason for that choice is twofold. First, it is more conservative to select a small dispersivity value that reduces dispersion and leads to a higher flux and concentration peaks. Second, the strong variability of the velocity field at and around the transition zone dominates the dispersion process rendering the local-scale dispersion effect very minor. In addition, the macrodispersivity used for the saltwater intrusion problem introduces an artificial dispersion process that compensates for neglecting the spatial variability of hydraulic conductivity.

The calibrated flow model at a grid scale of about 100 m is used to perform random walk particle-tracking experiments for which there is no lower limit for the local dispersivity value that can be used. The longitudinal local dispersivity, α_L, is thus changed from a minimum of about 0.56 m to a maximum of 19.5 m. The 100-value distribution that is generated from a lognormal distribution has a mean of about 5.0 m and is shown in Figure 4.8. Transverse local dispersivity, α_T, is taken as one tenth of the longitudinal value. Again, these 100 simulations are performed using a single FEFLOW output for the purpose of analyzing the effect of local dispersivity alone.

The last parameter to be analyzed within transport simulations is the matrix diffusion parameter, κ. Based on the discussion of Section 3.2.3, a best estimate for κ of 1.37 $day^{-1/2}$ was derived (consistent with θ_m of 0.12, b of 5.0×10^{-4} and D_m* of 3.2745×10^{-5} m^2/day). This value leads to a very strong diffusion into the matrix, which significantly delays the mass arrival to the seafloor, producing no mass breakthrough at the seafloor within the selected time frame of about 27,400 years of this first modeling stage. As there is a large degree of uncertainty in determining this parameter manifested in the uncertainty in b and D_m*, and there is uncertainty derived by the conceptual model assumptions for diffusion (*e.g.*, assumption of an infinite matrix), values for κ that are smaller than the best estimate of 1.37 were chosen. A random distribution of 100 values is generated for κ with a minimum of 0.0394, a maximum of 1.372 and a mean of 0.352. This mean

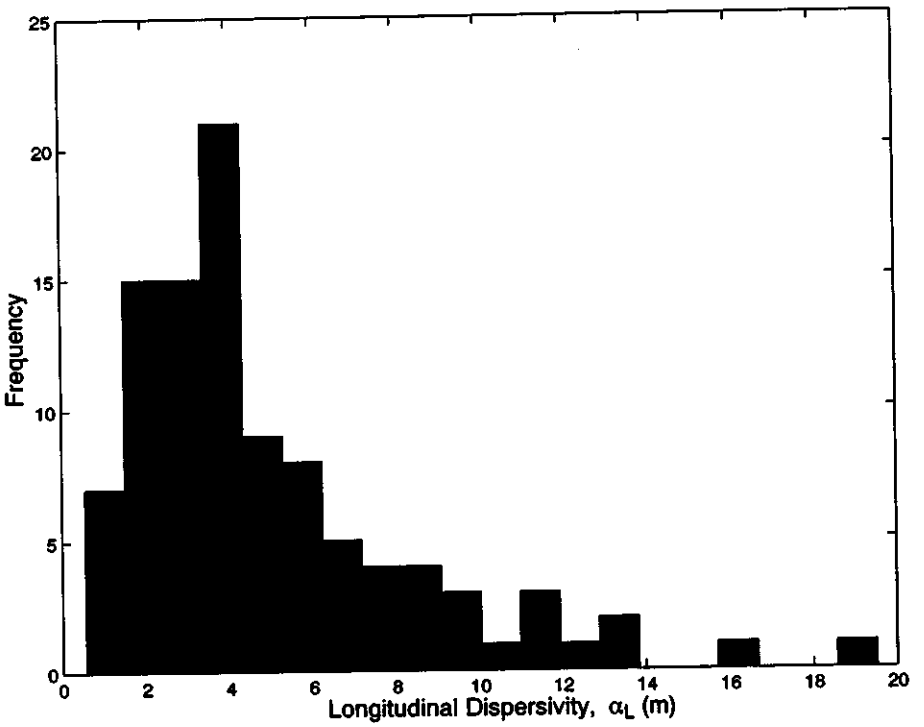

Figure 4.8. Randomly generated distribution for longitudinal local dispersivity for the first modeling stage.

is close to the κ value of 0.434 that is obtained from the same parameters described above for its best estimate, but using an order-of-magnitude-lower diffusion coefficient. The lower end of the distribution is yet another order-of-magnitude-lower κ. Figure 4.9 shows the distribution of these values and the effect on the retention function, $\gamma(t, \tau)$, that is used for matrix diffusion computation. The distribution shown in Figure 4.9 is generated from a lognormal distribution with a standard deviation adjusted to a minimum and a maximum value close to the ones specified above. The difference between these two extremes is very significant as depicted by the lower plot of Figure 4.9. This plot shows how the retention function behaves with different κ values. As can be seen, the function has a lower peak and a much longer tail for higher values of κ. This function indicates that if there is a single pulse of conservative (and no matrix diffusion) mass flux crossing the seafloor at time τ = 1,000 days within a time step of Δt and with unit value, the mass flux after including the matrix diffusion effect is given by $\gamma(t, \tau) \times \Delta t$. This implies that $\int_0^\infty \gamma(t,\tau)dt = 1.0$ for any value of τ.

The analysis here is performed using a single flow realization and a single particle-tracking realization with the mean values of transport parameters (α_L=5.0 m and $k_g = 1.26 \times 10^{-7}$ days^{-1}). The conservative breakthrough of this realization is convoluted with the γ function (Equation 3.14) for 100 realizations of the parameter κ that are generated as discussed above. The resulting 100

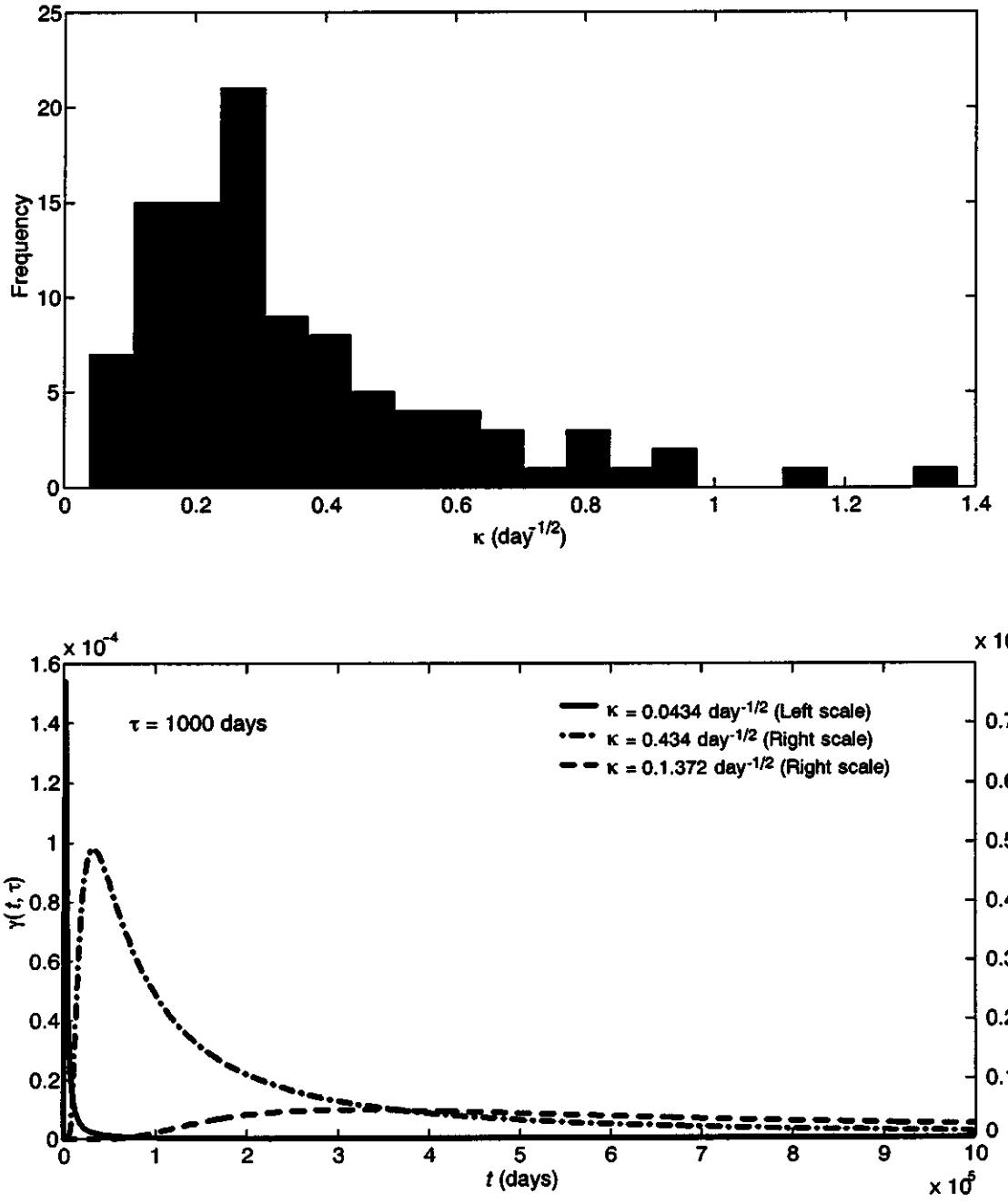

Figure 4.9. Randomly generated distribution for the matrix diffusion parameter, κ (top), and the dependence of the retention function, γ, on the value of κ (bottom).

breakthrough curves are analyzed for arrival time and location of the breakthrough with respect to the bathymetric profile.

4.3 Results of the Parametric Uncertainty Analysis

The transport modeling described in the previous section is applied to the four cases dealing with flow parameters, and the results of the 100 Monte Carlo realizations for each parameter are analyzed in terms of mean arrival time and location of breakthrough. For all these cases, the particle-tracking experiments are performed with a time step of 100 days and for a total simulation time of 10^7 days (27,400 years). Transport parameters such as glass dissolution, local dispersivity and matrix diffusion parameter are kept unchanged in all these cases. Longitudinal and transverse local dispersivities, α_L and α_T, are taken as 5.0 m and 0.5 m, respectively, and matrix diffusion parameter, κ, is fixed at 0.434 and 0.0434 days$^{-1/2}$. In each case, 100 conservative, total mass flux, $Q(t)$, breakthrough curves are obtained and then convoluted with the matrix-diffusion gamma function of Equation (3.14) to yield the undecayed breakthrough curves for a 100% hydraulic release scenario. Due to the matrix diffusion effect, the mass that breaks through within the time frame of 27,400 years is far less than 100% of the total mass released within the cavity. Therefore, the breakthrough curves are analyzed in terms of the mean arrival time of the mass that breaks through within this time frame and the location of this breakthrough along the bathymetric profile. Recall that the purpose of this analysis is to select the parameters for which the associated uncertainty has the most significant effect on transport results expressed in terms of uncertainty of travel time to the seafloor and the location where breakthrough occurs. By doing so, the parameters for which the uncertainty only slightly affects the uncertainty in travel time and transverse location of the breakthrough can be identified, and as such these parameters are fixed at their best estimate and only those with significant effects are varied.

In addition to the four parameters discussed here (*Rech*, K, θ, A_L), the results using the case with randomly chosen conductivity but with a porous medium porosity of 0.12 are also presented. This porosity value is the average of all the core measurements for the Kirilof Point and Older Breccias formations. The objective is to compare a case with a very low fracture porosity and matrix diffusion to a case with a continuum porous medium that has no matrix diffusion, but a large porosity value. In the porous medium case, the whole domain including the cavity and chimney is assigned a uniform porosity of 0.12. The 100 conservative breakthrough curves are then analyzed in a manner similar to the other cases described above.

The results of the sensitivity analysis performed for the seven parameters, K, *Rech*, θ, A_L (in saltwater intrusion), k_g, α_L (in radionuclide transport modeling) and κ are summarized in Table 4.1a and Table 4.1b. The difference between the tables is that the matrix diffusion parameter,κ, is assigned the base-case value of 0.434 day$^{-1/2}$ in Table 4.1a and the sensitivity value of 0.0434 day$^{-1/2}$ in Table 4.1b. In addition, the random conductivity case with porous medium porosity is also presented in Table 4.1a. For each case, the table presents the range of values of the input parameter (minimum, maximum and mean), the standard deviation, and the coefficient of variation. On the output side, the results are presented in terms of the statistics of travel time and transverse location

Table 4.1a. Results of the parametric uncertainty analysis for Milrow comparing the effects of different parameters on plume travel time and transverse location of the breakthrough. The matrix diffusion coefficient, κ, is 0.434, except where uncertainty in κ is evaluated. Dashes indicate where statistics could not be computed due to lack of breakthrough.

Input Statistics						Output Statistics						
						Travel Time (10^3 years)			Transverse Location (km)			# of Realizations
Parameter	Min	Mean	Max	σ	cv	Mean	σ	cv	Mean	σ	cv	
K (m/d) (fracture flow)	0.888×10^{-3}	6.77×10^{-3}	2.445×10^{-2}	4.34×10^{-3}	0.641	-	-	-	-	-	-	0
Rech	0.328	1.125	2.2047	0.475	0.422	26.518	0.313	0.012	3.770	0.118	0.032	18
A_L (m) salt water intrusion	62	300	500	82	0.272	-	-	-	-	-	-	0
θ	1.294×10^{-3}	5.2×10^{-3}	3.8×10^{-3}	6.38×10^{-4}	1.227	24.456	2.890	0.118	3.334	0.077	0.023	36
a_L (m) transport	0.56	5.00	19.5	3.45	0.690	-	-	-	-	-	-	0
k_g (day^{-1})	1.56×10^{-8}	2.44×10^{-7}	2.54×10^{-6}	3.32×10^{-3}	1.360	-	-	-	-	-	-	0
κ (day^{-1})	0.0394	0.352	1.37	0.243	0.691	25.770	1.150	0.045	3.274	0.031	0.009	27
K (m/d) (porous medium flow)	0.888×10^{-3}	6.77×10^{-3}	2.445×10^{-2}	4.34×10^{-3}	0.641	230.400	85.000	0.368	3.129	0.247	0.079	29

Table 4.1b.Results of the matrix diffusion sensitivity modeling comparing the effects of different parameters on plume travel time and transverse location of the breakthrough when the matrix diffusion parameter, κ, is 0.0434 rather than the base-case value of 0.434.

Input Statistics						Output Statistics						
						Travel Time (10^3 years)			Transverse Location (km)			# of Realizations
Parameter	Min	Mean	Max	σ	cv	Mean	σ	cv	Mean	σ	cv	
K (m/d) (fracture flow)	0.888×10^{-3}	6.77×10^{-3}	2.445×10^{-2}	4.34×10^{-3}	0.641	22.188	1.980	0.089	3.629	0.660	0.182	98
Rech	0.328	1.125	2.2047	0.475	0.422	22.000	3.484	0.158	3.404	0.375	0.110	90
A_L (m) salt water intrusion	62	300	500	82	0.272	20.650	0.742	0.036	3.394	0.009	0.003	100
θ	1.294×10^{-3}	5.2×10^{-3}	3.8×10^{-3}	6.38×10^{-4}	1.227	19.101	4.965	0.260	3.382	0.042	0.012	97
α_L (m) transport	0.56	5.00	19.5	3.45	0.690	23.076	0.309	0.013	3.366	0.024	0.007	100
k_g (day^{-1})	1.56×10^{-8}	2.44×10^{-3}	2.54×10^{-6}	3.32×10^{-3}	1.360	23.205	0.300	0.013	3.362	0.036	0.011	100

where breakthrough occurs. For each single realization of the radionuclide transport, the mean arrival time and mean transverse location of the mass that has crossed the seafloor within 27,400 years are recorded. This time frame is used for all cases except the porous medium (no fracture flow) scenario, where the simulation time is about 5,480,000 years. The resulting ensemble of these values is used to compute the mean, standard deviation and coefficient of variation of the travel time and location. These values are presented in Table 4.1a and Table 4.1b along with the number of realizations (out of 100) that show mass breakthrough within the above-mentioned time frames. The mean arrival time for the case of K in porous medium flow is significantly larger than the other cases due to the longer simulation times considered for this case.

To facilitate the comparison between different cases, one would compare the values of the coefficient of variation on both input and output sides. The case of random conductivity but with a porous medium conceptualization shown in Table 4.1a is only presented for comparison purposes. Comparing this case to the similar fracture flow case where matrix diffusion is added ($\kappa = 0.0434$, Table 4.1b) indicates that the addition of matrix diffusion reduces some of the variability in the plume arrival time. Although the simulation time for the porous medium scenario is about 5.5 million years, only 29 realizations show some mass breakthrough. This is attributed to the very small flow velocities when using a uniform porous medium porosity of 0.12. The porous medium scenario will not be considered in any further analysis.

Table 4.1a shows that none of the 100 realizations considered showed any breakthrough with $\kappa = 0.434$ day$^{-1/2}$ for the cases addressing uncertainty in K, A_L, α_L, and k_g. This is essentially due to the strong effect of matrix diffusion with $\kappa = 0.434$ day$^{-1/2}$. Recharge uncertainty leads to some uncertainty in arrival times, which is the least compared to θ and κ uncertainty cases (Table 4.1a). To avoid the complete elimination of mass by matrix diffusion, which hinders the statistical analysis of arrival times, we present the uncertainty effects using $\kappa = 0.0434$ day$^{-1/2}$ in Table 4.1b.

Among the six cases in Table 4.1b, the two cases encountering variability in the macro/local dispersivity value lead to very small uncertainty in the travel time and the transverse location in comparison to other parameters. Although the coefficient of variation of α_L in radionuclide transport simulations is higher than that of conductivity and recharge, the resulting coefficients of variation for travel time and transverse location are much smaller. The glass dissolution coefficient, k_g, encounters the largest variability (coefficient of variation is 1.36), yet the effect on travel time and transverse location is minor as compared to conductivity and recharge. Therefore, it can be argued that the uncertainty in these three parameters may be neglected as their variabilities slightly influence transport results when compared to other parameters. This leaves the four parameters, K, *Rech*, θ, and κ. The fracture porosity variability with the highest coefficient of variation among these four parameters leads to the highest variability in mean arrival time. The conductivity on the other hand leads to the highest variability in transverse location. The first three parameters of this reduced list influence the solution of the flow problem and thus require multiple realizations of the flow field. The matrix diffusion parameter is a transport parameter that does not require multiple flow realizations.

The final choices for the uncertain parameters for the second modeling stage are the three flow parameters. The uncertainty of the matrix diffusion parameter will be assessed in a less rigorous manner within a simple sensitivity analysis. This choice is motivated by the fact that we only have data pertinent to the solution of the flow problem, which can be used to guide the generation of the random distributions in the second stage. Head and chloride concentration data can be used as criteria for determining whether the combined random distributions lead to realistic flow solutions or not. Given that using the same random distribution for κ as in the first stage or skewing it towards higher or lower values cannot be judged or tested against data, the transport results using a different κ value are compared in the sensitivity section.

THIS PAGE LEFT INTENTIONALLY BLANK